Integration of multiscale porosities and permeabilities in Paleogene reservoir rocks of the Middle Magdalena Valley Basin, Colombia

Integración de porosidades y permeabilidades a múltiples escalas en rocas reservorio del Paleógeno en la Cuenca del Valle Medio del Magdalena, Colombia

Ricardo Amorocho-Parra [a]**; Carlos Alberto Villarreal-Jaimes** [a]**; Jorge Arley Meza-Ortíz** [a]**; Carlos Alberto Ríos-Reyes** [a]

[a] *Universidad Industrial de Santander, Escuela de Geología, Bucaramanga, Colombia; Mail: amorocho.ricardo@gmail.com; geoalbertovilla@gmail.com; jorgearley.meza@gmail.com; carios@uis.edu.co*

Correspondence: *carios@uis.edu.co*

Abstract

This study presents a descriptive mineralogical and textural analysis of sedimentary rocks located at the top of Paleogene formations in the Middle Magdalena Valley Basin, specifically within the La Paz, Esmeralda, Colorado, and Mugrosa formations. These units exhibit clearly distinguishable sedimentary structures, depositional environments, and mineral compositions. Advanced techniques such as X-ray computed tomography (CT), petrography, X-ray diffraction (XRD), and scanning electron microscopy (SEM) were used to thoroughly characterize the sedimentological, mineralogical, and porosity properties of the samples. X-ray CT enabled the identification of sedimentary and biogenic structures, as well as syn-sedimentary deformations, and provided density and effective atomic number values that are useful for facies differentiation. Petrographic analysis revealed sandstones with variable grain sizes, typical of fluvial environments, showing significant variations in grain size, a wide range of cementing materials, and well-developed secondary porosity that enhances reservoir permeability. XRD identified quartz, feldspars, and clay minerals as the main components, while SEM highlighted the distribution of clay minerals within the pores. The observed lithologies include polymictic conglomerates, shales, sandy shales, sublithic sandstones, and lithic sandstones, associated with fluvial channels, floodplains, and meandering river systems. Computed tomography is consolidated as a key non-destructive tool in sedimentological interpretation, offering high-resolution imaging and valuable data on density, mineralogy, lithology, porosity, and facies. This multidisciplinary approach provides essential information for reservoir characterization, the reconstruction of depositional environments, and the understanding of geological history, contributing to the advancement of geological research and resource exploration in the Middle Magdalena Valley Basin.

Resumen

Este estudio realiza un análisis descriptivo mineralógico y textural de las rocas sedimentarias ubicadas en los topes formacionales del Paleógeno en la cuenca del Valle Medio del Magdalena, específicamente en las formaciones La Paz, Esmeralda, Colorado y Mugrosa. Estas unidades muestran estructuras sedimentarias, ambientes de depósito y composiciones minerales claramente diferenciables. Se utilizaron técnicas avanzadas como tomografía computarizada (TC) por rayos X, petrografía, difracción de rayos X (DRX) y microscopía electrónica de barrido (MEB) para caracterizar detalladamente las propiedades sedimentológicas, mineralógicas y de porosidad de las muestras. La TC por rayos X permitió identificar estructuras sedimentarias, biogénicas y deformaciones sin-sedimentarias, además de proporcionar valores de densidad y número atómico efectivo útiles en la diferenciación de facies. El análisis petrográfico mostró areniscas con granulometría variable, típicas de ambientes fluviales, con importantes variaciones en el tamaño de grano, diversidad de cementos y desarrollo de porosidad secundaria, lo cual mejora la permeabilidad del reservorio. La DRX identificó cuarzo, feldespatos y minerales arcillosos como componentes principales, mientras que la MEB evidenció la distribución de minerales arcillosos en los poros. Las litologías observadas incluyen conglomerados polimícticos, lutitas, lutitas arenosas, sublitosandstones y litosandstones, asociadas a canales fluviales, llanuras de inundación y ríos meandriformes. La tomografía computarizada se consolida como una herramienta no destructiva clave en la interpretación sedimentológica, al ofrecer imágenes de alta resolución y datos sobre densidad, mineralogía, litología, porosidad y facies. Este enfoque multidisciplinario aporta información esencial para la caracterización de yacimientos, la reconstrucción de ambientes deposicionales y la comprensión de la historia geológica, contribuyendo al avance en la investigación geológica y la exploración de recursos en la cuenca del Valle Medio del Magdalena.

Keywords: clay minerals; petrophysical properties; reservoirs; sedimentary sequences; Colombia.

Palabras clave: minerales arcillosos; propiedades petrofísicas; reservorios; secuencias sedimentarias; Colombia.

1. Introduction

The application of X-ray computed tomography (CT) imaging to the porous system of reservoirs of sedimentary rocks has been used for many years to study and understand their petrophysical properties [1-2]. X-ray CT imaging is a powerful non-destructive technique [3-8] used in the oil industry to evaluate the internal structures of cores. The acquisition of high-resolution continuous images along the core length is essential in complex reservoirs to characterize reservoir heterogeneity and optimize sample selection for further detailed analysis [9]. It produces continuous whole core scans at 0.5mm spacing to obtain logs for bulk density (RhoB) and effective atomic number (Zeff), which are very useful to determine quantitatively bulk mineralogy data, lithology, porosity and rock facies [9-10]. The principles of X-ray CT have been discussed extensively elsewhere [3,11-12], and its application to rock reservoirs has been used for many years to study and understand their petrophysical properties [1-2,13]. The petrophysical properties of rock reservoirs as well as storage and fluid flow are of paramount importance in the assessment and management of these reservoirs and play a fundamental role in optimizing the recovery of natural resources. These properties, ranging from porosity and permeability to fluid saturation, are critical in a reservoir's capacity to host and produce hydrocarbons or fluids. Understanding petrophysical properties is essential in evaluating a reservoir's storage efficiency and predicting how fluids will behave within it. Furthermore, these properties are important in planning extraction and decision-making in the oil and gas industry. Towards the end of the 20th century, a series of works began to be published that focused on the application of X-ray CT imaging in the identification and interpretation of sedimentological characteristics, such as sedimentary structures, framework and fabric, which was primarily targeted to sand and carbonate-bearing rocks [8,14-17].
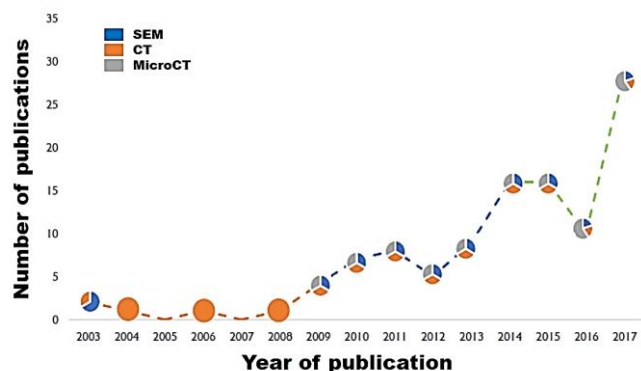

Figure 1. Scientific production reflected in publications over time and with the use of SEM (Scanning Electron Microscope), TC (Computer Tomography) and MICRO TC (Micro Computer Tomography) techniques. Adapted and modified from García and Marin [18].

In Colombia, the published works on the use of the technique for sedimentological interpretation are scarce or null, although in the oil industry it has been used for a decade to obtain information on the petrophysical properties and recently to study the fluid-rock interaction in rock reservoirs. Worldwide, the rise of the technique is taking a very important place reflected in the publications of recent years (Figure 1).

This work seeks to show the advantages of the X-ray CT technique, to identify sedimentological characteristics in digital rock results, mainly textural characteristics and sedimentary structures (primary, secondary and/or biogenic) that facilitate the definition of sedimentary X-ray CT facies. Finally, with the integration of X-ray CT and conventional petrography information, it is sought to carry out a sedimentological analysis and establish its possible scope in the definition of facies and in the identification of characteristics of the sedimentary deposit. The purpose of this paper is to propose a workflow on the integration of X-ray CT with conventional petrography (transmitted light microscopy) and scanning electron microscopy for the description and interpretation of sedimentological characteristics in siliciclastic and calcareous sedimentary rocks.

2. Geological setting

The siliciclastic and calcareous sandstone samples were taken from the Paleogene La Paz, Esmeralda, Colorado and Mugrosa formations (their stratigraphic limits are not the subject of study), considering that they are the main Paleogene units, producers of hydrocarbons in the petroleum system from the Middle Magdalena Valley (MMV) basin (Figure 2). Next, we briefly recount the main characteristics of the lithostratigraphic units sampled and the main structures that outcrop in the study area. From base to top, the sequence consists of rocks of middle Eocene age, designated as the La Paz Formation. At the base, it begins with a layer of polymictic conglomerate, followed by mudstones and bioturbated sandy mudstones, transitioning into sublitharenites and litharenites. The bedding is inclined upwards, with an increase in grain size. This trend reverses as the Esmeraldas Formation is reached at the top, where the facies show a decrease in grain size, exhibiting a cyclical pattern influenced by fluvial environments, including channels and floodplains, primarily braided rivers. Overlying these rocks are the Esmeraldas and Colorado formations, dating from the Oligocene-Miocene, composed of muddy sandstones, primarily subarkosic to arkosic, slightly calcareous, and deposited in meandering river (point-bar) and floodplain conditions [19-21]. These lithostratigraphic units are in contact on the Paleocene rocks through a regional erosive unconformity. It is common to find some levels of paleosols, as well as unconformable surfaces of a local nature. The main structure corresponds to the New World

Syncline, which is cut by different faults, in this sector the syncline is cut by the Lebrija Fault, of an inverse type with a sinistral strike component, cutting the eastern flank [22].
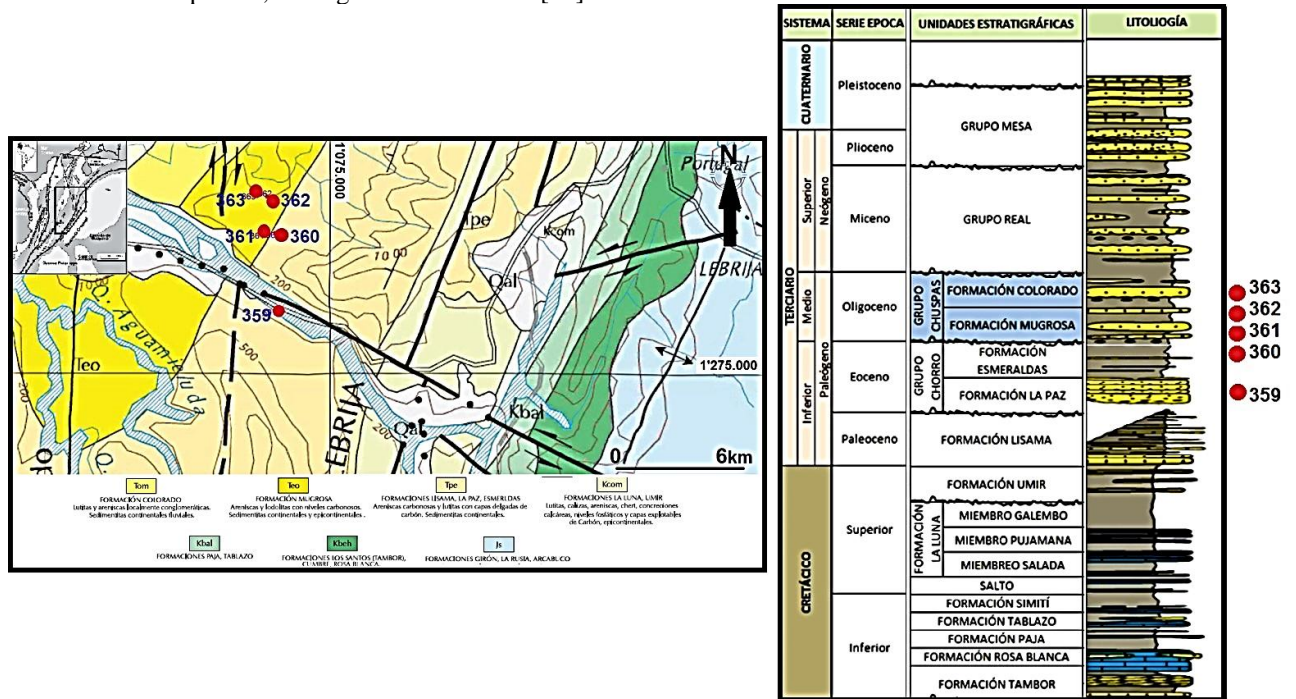

Figure 2. Left, geological map of the study area. Source: Modified from INGEOMINAS [23]. Right, generalized stratigraphic column of the MMV basin. Source: Adapted and modified from Barrero et al. [24]. The red dots indicate the sampling sites.

3. Materials and methods

Siliciclastic and calcareous sandstone samples of interest in this study were collected from outcrops of the Paleogene La Paz, Esmeralda, Colorado, and Mugrosa formations. Researchers obtained five sandstone cores (5.08 cm in diameter and 7-11 cm in length) using a pneumatic drill at the Geological Samples Preparation Laboratory of the School of Geology at Universidad Industrial de Santander, where they also prepared thin sections for petrographic analysis. The samples were cut transversely, and the thin sections, made to standard size (47 mm x 27 mm x 1.0 mm), were impregnated with blue-tinted epoxy resin to enhance porosity. Likewise, each thin section has stains to highlight the presence of potassium feldspar and differentiate carbonates according to their iron content. Petrographic analysis was performed using transmitted light microscopy with a Nikon trinocular microscope, model Labophot2-POL. The thin sections were first examined under parallel and crossed nicols to obtain preliminary information, which was essential for identifying areas of interest for microphotography. This inspection allowed the determination of textural parameters, such as the degree and direction of lamination, and the degree of bioturbation, characterized using the Bioturbation Index (BI) proposed by Reineck [25] and later modified by Taylor and Goldring [26]. Additionally, the analysis covered grain size, sorting, roundness, and the contact between grains for terrigenous components, as well as the mineralogical composition, primary and secondary porosity, and the diagenetic processes that affected the rock. For the classification of the sandstones, the ternary diagrams proposed by Folk [27] were used, according to the classifying minerals Q-F-L (quartz-feldspar-rock fragments), for composition and G-S-M (gravel-sand-mud) and A-Arc-L (sand-clay-silt) for texture. Rudites are classified texturally in the sense of Folk [27], compositionally according to Pettijohn [28] and Limarino *et al*. [29]. For the qualitative classification of pore sizes, the pore size classification and its relationship with the Udden-Wentworth [30] scale will be used. The textural classification used for fine-granular rocks is the one proposed by Picard [31] and compositional by Folk [27]. Bulk mineralogical composition was determined via X-ray powder diffraction (XRPD) using a BRUKER D8 ADVANCE X-ray diffractometer equipped with operating in Da Vinci geometry and equipped with an X-ray tube (Cu-Kα1 radiation: λ = 1.5406 Å), a 1-dimensional LynxEye detector (with aperture angle of 2.93º), a divergent slit of 0.6 mm, two soller axials (primary and secondary) of 2.5° and a nickel filter. All samples were milled in an agate mortar to a particle size of less than 38 μm (400 mesh) and then mounted on a sample holder of polymethylmethacrylate (PMMA) using the filling front technique prior to XRPD analysis. Data collection was carried out at 40 kV and 40mA in the 2θ range of 2-70°, with a step size of 0.02035° (2θ) and counting time of 0.6 s/step. Phase identification was performed using the

crystallographic database Powder Diffraction File (PDF-2) from the International Centre for Diffraction Data (ICDD) and the Crystallographica Search-Match program. The quantitative analyzes of the mineral phases were performed by fitting between the observed XRPD profiles and those reported in the Inorganic Crystal Structure Database using the Rietveld method. The percentages reported correspond to the relationship between the polycrystalline phases without considering the percentage of amorphous material. The pore morphology and elemental composition of freshly broken surfaces of samples were analyzed by field emission gun-environmental scanning electron microscopy/energy dispersive X-ray spectroscopy (FEI QUANTA 650 FEG-ESEM/EDS) under the following analytical conditions: magnification = 200-8000x, WD = 14.9-15.1 mm, HV = 25 kV, signal = BSED in ZCONT mode, detector = BSED, EDS Detector EDAX APOLO X with resolution of 126.1 eV (in. Mn Kα). All the samples were carbon coated for observation. The effective porosity was obtained in a Core-Pet brand Helium porosimeter, by the Boyle method and the unit of measure of the analyzed variable is expressed in percentage (%), while the permeability was obtained in a Core-Pet brand semi-automated permeameter by the steady state method expressed in milli Darcy (mD). The computed tomography was performed on a dual energy GENERAL ELECTRIC brand equipment with two second generation energies in plugs (resolution of 0.5 mm), 1830 cuts / mt, apparent density, atomic number, circumferential view, porosity, lithotypes. In this study, we present a comprehensive workflow designed to extract maximum information from various analytical techniques, including X-ray CT, conventional petrography, XRPD, and SEM. The integration of these methods is important for a holistic understanding of sedimentary rocks. Identifying the pertinent information from X-ray CT results is very important, and researchers strategically incorporate this information into sedimentological analyses alongside conventional petrography. The proposed workflow, illustrated in Figure 3, is devised to capitalize on the capabilities of X-ray CT, generating high-resolution images of rock samples. These images serve as a basis for identifying specific features within the samples, contributing significantly to sedimentological interpretations. Moreover, the workflow includes an assessment of the potential applicability of RhoB and Zeff values in delineating textural and compositional parameters. By combining the strengths of X-ray CT with traditional petrographic techniques, we aim to enhance the overall sedimentological analysis. The workflow not only streamlines data acquisition but also facilitates a detailed examination of the rock's internal structures. This integrated approach holds the key to unlocking valuable insights into the sedimentary structures of the investigated sandstones, shedding light on the depositional conditions and geological processes that shaped these rocks.
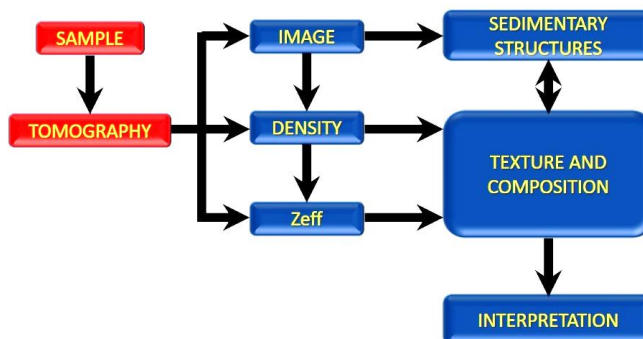

Figure 3. Workflow proposed as a methodology for the sedimentological interpretation of X-ray CT results. Source: Authors.

From the X-ray CT images, the information that should be highlighted mainly are the geometries formed by the sedimentary structures, as well as the deformations due to compaction processes, biodisturbance or tectonism events (fractures, joints and/or faults). Based on the RhoB and Zeff values obtained from X-ray CT, we can propose a possible interpretation of the rock's composition and texture. This interpretation can also be linked to the percentages of framework and matrix in clastic sedimentary rocks, using approximate values for known rocks and minerals (Table 1). For example, sedimentary structures such as ripples are unlikely to occur in rocks with grain sizes larger than 0.25 mm (under low to moderate flow velocity conditions). Similarly, laminations or structures formed by suspension transport will not form in rocks with grain sizes greater than 0.125 mm, which typically occurs under laminar flow conditions [27]. With this analysis, it is possible to propose a X-ray CT facies nomenclature or facies codes (the number of X-ray CT facies codes depends on the number of samples and their sedimentological complexity), which can help identify specific characteristics of the deposit. From these associations, we can approximate the conditions under which the sedimentary deposit formed.

The X-ray CT images record the differences in the degree of attenuation of the X-rays, which is dependent on the material and the energy level implemented, mainly due to the interactions of photoelectric absorption and Compton absorption. The contribution of the photoelectric effect depends on the effective atomic number and occurs mainly at low radiation energies. At high energies, the Compton effect prevails, and the attenuation is mainly determined by the density of the material.

To transform X-ray CT numbers into RhoB for the examined cores, Wellington and Vinegar [36] suggested employing a calibration curve, a concept illustrated in detail in Figure 4. This curve relies on clean sandstone samples, serving as key "standards", each characterized by known, measured RhoB obtained from diverse quarries or reservoirs. Although this approach generally produces satisfactory results, it is worth emphasizing the importance of scanning these standards in an environment congruent with the actual cores, particularly

when dealing with preserved cores, as pointed out by Siddiqui [37]. This additional step serves as a precautionary measure aimed at preventing the necessity for subsequent adjustments. Ensuring that the standards and preserved cores share the same scanning environment not only enhances the reliability of the RhoB conversions but also contributes to the overall precision of the analytical process. This alignment in scanning conditions helps mitigate potential discrepancies,

ultimately reinforcing the accuracy and robustness of the RhoB-to-X-ray CT number transformations for a more reliable geological interpretation

Table 1. Density values for some minerals, which are commonly identified by X-ray CT. Source: Adapted and modified from previous studies [33-35].

| Mineral		Density	Mineral		Density
Quartz	SiO_2	2.65-2.66	Illite	$(K,H_3O)(Al,Mg,Fe)_2(Si,Al)_4O_{10}[(OH)_2,(H_2O)]$	2.60-2.90
K-feldspar	$K_2OAl_2O_3.6H_2O$	2.54-2.63	Calcite	$CaCO_3$	2.69-2.71
Plagioclase	$NaAlSi_3O_8\text{-}CaAl_2Si_2O_8$	2.60-2.76	Dolomite	$CaMg(CO_3)_2$	2.84-2.86
Muscovite	$KAl_2(AlSi_3O_{10})(OH)_2$	2.77-2.88	Siderite	$FeCO_3$	3.80-3.96
Biotite	$K(Mg,Fe)_3AlSi_3O_{10}(OH,F)_2$	2.70-3.30	Anhydrite	$CaSO_4$	2.20-2.98
Phlogopite	$K(Mg,Fe,Mn)_3Si_3AlO_{10}(F,OH)_2$	2.78-2.85	Gypsum	$CaSO_4 \cdot 2H_2O$	2.30-2.37
Chlorite	$(Mg,Fe)_3(Si,Al)_4O_{10}(OH)_2(Mg,Fe)_3(OH)_6$	2.60-3.30	Halite	$NaCl$	2.04-2.17
Kaolinite	$Al_2Si_2O_5(OH)_4$	2.60-2.63	Zeolite Group	$M^{n+}_{1/n}(AlO_2)-(SiO_2)_x \cdot yH_2O$	2.05-2.35
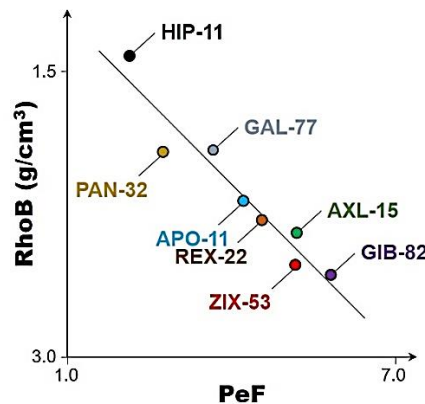
Figure 4. Above, calibration set, with different types of rock for scanning geological materials. Below, Bulk Density (RhoB) vs. Photoelectric Factor (PeF) cross-plot of different rock types. Source: Authors.

4. Results

4.1. X-ray Computed Tomography

It is important to consider the limitations posed by the limited data, as each sample represents only a small portion of the lithostratigraphic thickness of the units studied. Additionally, the samples come from intervals of different

chronostratigraphic ages, as reported in the literature, and are consistent with previous studies on the rocks in this sector of the MMV [19-20], although the interpretation obtained from the methodological proposal is incorporated. One of the important considerations when working with X-ray CT and rock data is the ability to utilize known equations and densities of certain materials to derive information about the

effective atomic number and the photoelectric factor. This enables the creation of graphs that illustrate the observed trends in the most common minerals, as detailed in Figure 5. The lithological contents of the Paleogene reservoir rocks of the Middle Magdalena Valley Basin (Colombia) were investigated using the combination of different logs cross-plot such as the RhoB vs. PeF and RhoB vs. Zeff in the studied sedimentary rocks.

The RhoB vs. PeF cross-plot (Figure 5a) shows that the data points of the reservoir rocks (represented by red dots) are concentrated on the sandstone line. The relationship between RhoB and PeF can be relevant in characterizing rock properties through X-ray CT. In sedimentary rocks, where composition can vary significantly, understanding this relationship can be essential. Evidently, the studied sandstones are essentially composed of quartz and other minor minerals with distinct properties. It can have applications in geological and paleontological research, helping identify sedimentary layers, internal structures, and possibly fossils. It's important to note that the interpretation of RhoB and PeF in rocks can be complex due to sample heterogeneity and variability in mineral composition. Additionally, the relationship between these two variables may depend on the X-ray energy used in tomography. Therefore, any specific analysis should consider the geological context and experimental conditions.

Figure 5b shows a RhoB vs. Zeff cross-plot and trend lines of the main minerals that reveal three distinct population clouds in the investigated sedimentary rocks; sandstones, argillaceous sandstones, and slightly argillaceous sandstone, which are low RhoB (high porosity) and low Zeff, and quartz-rich rock types. Furthermore, it mainly reflects the presence of quartz-rich sandstones. Certain patterns reveal key information about the physical properties and composition of these sedimentary rocks. The location of points in areas of lower RhoB and Zeff on the graph can be interpreted as indicative of sandstone porosity. These regions suggest empty spaces within the rock matrix, indicating the presence of pores that may contain fluids or gases. On the other hand, areas with higher values of RhoB and Zeff could suggest the presence of mineral cement. This phenomenon is related to the consolidation of sand grains by mineral substances, reducing porosity and providing greater cohesion to the rock. Quartz, with its characteristic profile of RhoB and Zeff, can visually cluster on the graph, standing out as a distinctive concentration. This pattern can be interpreted as a signal that quartz is the dominant mineral in the composition of the studied sandstones. Notable changes in point dispersion on the graph may suggest diagenetic alterations. These changes may result from geological processes that have altered the mineral composition of sandstones over time. For example, the selective dissolution of certain minerals or the precipitation of new components can leave a visual footprint on the graph, providing clues about the geological history of the sandstones. Furthermore, the RhoB

vs. Zeff cross-plot presents data on RhoB and Zeff for a selection of minerals (kaolinite, quartz, dolomite, illite, and calcite). The RhoB provides insights into the mass per unit volume of these minerals. Understanding mineral densities is important for tasks such as rock characterization, where variations in RhoB can indicate compositional changes or the presence of specific minerals. These values play a significant role in the interpretation of geological data, helping geologists identify and differentiate minerals within rock formations. The Zeff is a critical parameter that describes how effectively a material interacts with X-rays and gamma rays. By comparing the Zeff of different minerals, researchers can distinguish between them based on their unique X-ray attenuation properties, aiding in the identification and mapping of mineral compositions within geological formations. These data also serve as a valuable reference for scientists and researchers working in diverse fields and not only provides essential data for the listed minerals but also shows their distinct characteristics, enabling more accurate and informed analyses of geological samples and contributing to advancements in our understanding of Earth's subsurface composition and structure.

These resulting data are fundamental for understanding the mineralogical composition and variability within the studied rock samples. It visually represents how the PeF and Zeff vary depending on the mineral composition of the rocks. This is essential for the identification and quantification of minerals present in rock samples, as different minerals exhibit specific properties reflected in these measurements. The referred cross-plots of the data are very useful since with the trend lines it is possible to establish quadrants of interest relating the type of material, petrophysical properties and in some cases porosity. It aids researchers and geologists in interpreting and analyzing tomography data more accurately, thus providing a better understanding of the structure and composition of the geological formations under study. Ultimately, this information contributes to significant advancements in reservoir characterization and decision-making related to the exploration and exploitation of natural resources.
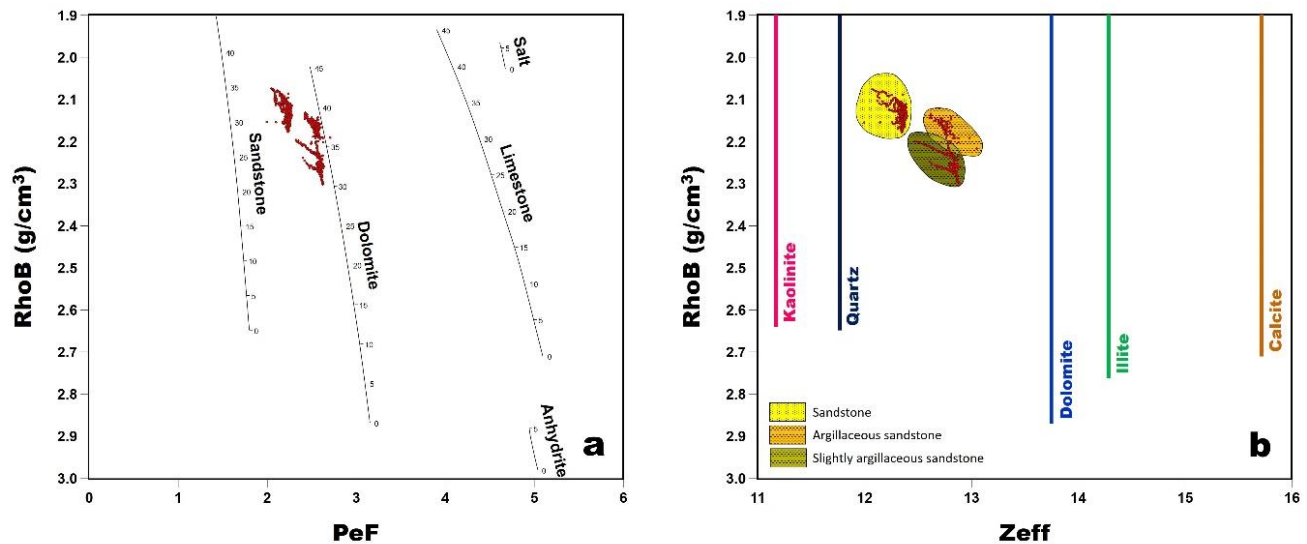
Figure 5. (a) Bulk Density (RhoB) vs. Photoelectric Factor (PeF) cross-plot. (b) Bulk Density (RhoB) vs. Effective Atomic Number (Zeff) cross-plot and trend lines of the main minerals. Source: Authors.

For each sample, an analysis of the information was carried out using the template shown in Figs. 6-10, where the results obtained from X-ray CT are integrated with the sedimentological interpretation. Each template has a scale in centimeters, the image of the sample with axial and radial sampling, the RhoB and Zeff curves, and followed by the sedimentological description columns. Distinguished by its exceptional resolution, X-ray CT can provide detailed images of geological samples at a fine scale. By harnessing the capabilities of X-ray CT, researchers can delve into the intricate details of geological specimens, unraveling the subtle features that might otherwise go unnoticed. The technique's ability to unveil the complex architecture of galleries and burrows is particularly noteworthy, providing a comprehensive understanding of the spatial distribution and morphological intricacies of these structures. In the realm of geological and paleontological research, the discernment facilitated by X-ray CT stands as a linchpin. The technique enables not only the detection but also the comprehensive recognition of diverse structures, such as galleries and burrows, unlocking a trove of information about past biological activities and prevailing environmental conditions. This nuanced insight proves invaluable, offering researchers a profound glimpse into the dynamic interplay between organisms and their surroundings throughout geological epochs.

The X-ray CT technique proves to be highly effective in discerning sedimentary and biogenic structures, as illustrated in Figure 6, where intricate galleries and burrows come to light. In the analyzed sample SR-1, two X-ray CT facies have been identified: Sm, representing compacted sandstone, and Sbio, indicative of sandstone with the presence of burrows or galleries. The presence of a compacted sandstone suggests that the sediments were deposited in an environment with enough energy to favor grain compaction. This could indicate the action of strong currents, waves, or tidal conditions, where water energy facilitated the compaction of sand grains. Compaction may result from diagenetic processes, which are physical and chemical changes that occur in sediments after their initial deposition. In this case, pressure from overlying sediment and the dissolution and redistribution of minerals can contribute to sandstone compaction. The presence of compacted sandstone could also indicate a significant cementation process. Minerals acting as cement fill the spaces between sand grains, hardening the rock. Cementation can result from mineral precipitation from aqueous solutions, such as mineral-rich groundwater. In some cases, the compaction of sandstone may be related to tectonic events. Tectonic movements can induce lateral pressures contributing to sediment compaction. Although compacted sandstone indicates it has undergone compaction processes, it can still be a porous rock. Compaction does not always result in a total loss of porosity, and the amount of retained porosity can influence the rock's ability to store and transmit fluids. The presence of burrows or galleries in sandstones often indicate the biological activity of marine or coastal organisms, such as worms, mollusks, or crustaceans. These organisms excavate burrows to seek food, shelter, or engage in reproductive activities. Their presence suggests that the rock formed in a marine or coastal environment. The type and abundance of burrows can provide information about the climate and environmental conditions at the time of deposition. The presence of burrows may suggest oxygen levels in the water during deposition. Organisms that create these structures often require oxygen, so the presence of burrows could indicate well-oxygenated environments. Variability in the RhoB and distribution of burrows could provide information about deposition cycles and fluctuations in environmental conditions over time. Periods of intense biological activity may coincide with specific moments in

sedimentary history. The presence of burrows can also influence the preservation of other fossils or biological remains in the rock, and they may act as conduits for the entry of sediments and minerals, contributing to the fossilization process.
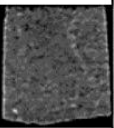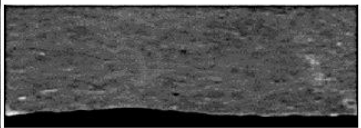

Figure 6. Above, X-ray circumferential view, RhoB, Zeff, structure and facies of sample SR-1. Below, plug of the referred sample, showing its textural and structural features. Note in the macroscopic image of the sample the excellent rock selection and some sectors with calcite cement and presence of oxides. No type of lamination is clearly observed. In the tomography image, the laminations and some biogenic structures can be clearly identified. Source: Authors.

In the examined sample SR-2 (Figure 7), three distinct X-ray CT facies have been identified, each offering unique insights into the sedimentary characteristics of the rock. The first facies, labeled as Sm, is represented by a compacted sandstone, which suggests deposition conditions with a high sediment load and pressure, leading to the compaction of sand grains. This could indicate deposition in a high-energy environment, such as a riverbed, deltas, or even in a marine setting with vigorous currents. The second facies, labeled as Sbio, is characterized by the intriguing presence of burrows or galleries, which suggests significant biological activity during sediment deposition. It indicates the presence of organisms, such as worms or crustaceans, that excavated structures in the sandstone while seeking food, shelter, or engaging in reproductive activities. This may point to a well-oxygenated marine or coastal environment. The third facies, labeled as Sx, unveils the presence of inclined planar or tangential lamination within the sandstone, which reveals complex structural patterns in the sandstone. This type of lamination suggests distinctive depositional processes, such as the influence of currents, changes in water flow velocity, or variations in sedimentary conditions over time. Therefore, these three facies could indicate a dynamic and complex sedimentary environment, where compaction, intense biological activity, and variations in depositional conditions contributed to the formation of the sandstone. This diverse set of features suggests a sedimentary history rich in events and environmental changes over time.
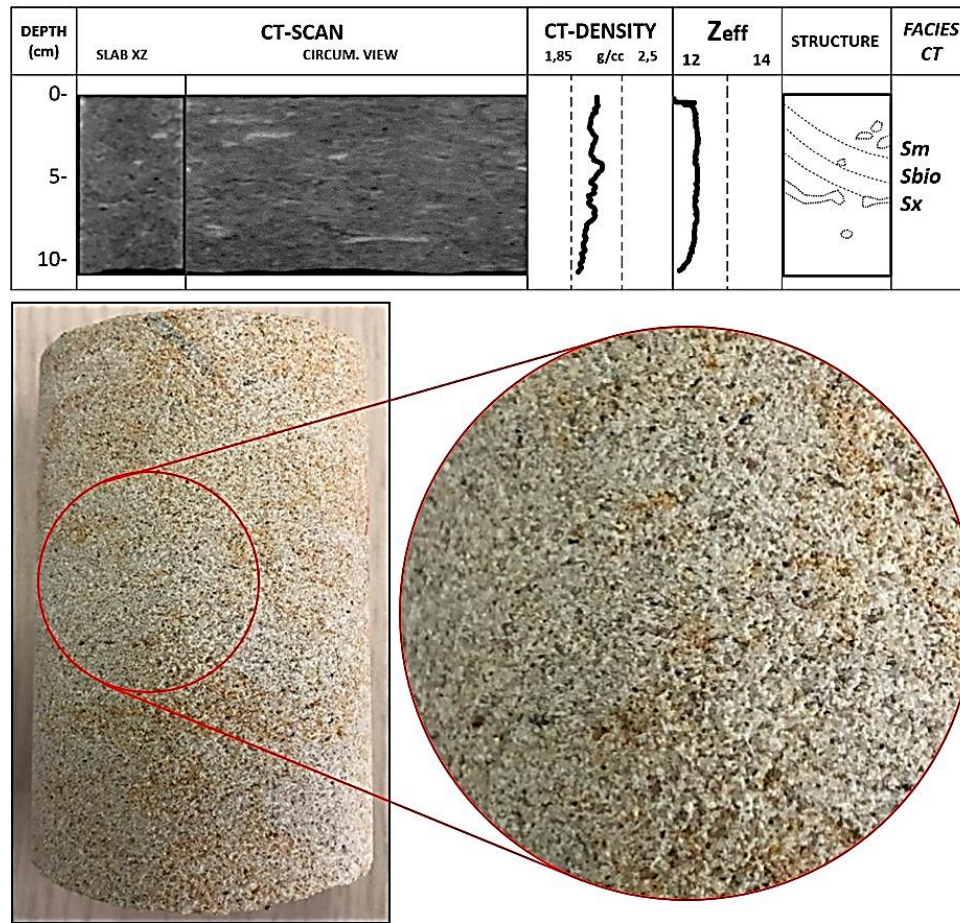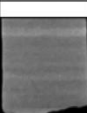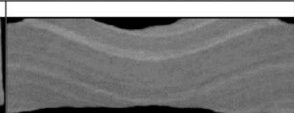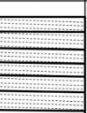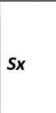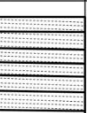
Figure 7. Above, X-ray circumferential view, RhoB, Zeff, structure and facies of sample SR-2. Below, plug of the referred sample, showing its textural and structural features. Note in the macroscopic image of the sample the excellent rock selection and some sectors with calcite cement and presence of oxides. No type of lamination is clearly observed. In the tomography image, the laminations and some biogenic structures can be clearly identified.
Source: Authors.

In the examined samples SR-3 (Figure 8) and SR-4 (Figure 9), only a singular and distinctive X-ray CT facies, labeled as Sx, reveals the presence of inclined planar or tangential lamination within the sandstone, which could indicate a specific sedimentary environment characterized by unique conditions during deposition, such as fluctuating currents or changes in water flow velocity. It is often associated with changes in depositional environment conditions over time. These changes may include fluctuations in water energy, variations in sediment load, or adjustments in flow direction. The exclusive presence of inclined lamination may provide clues about the dynamics of the sedimentary basin in which the sandstone was deposited. It might reflect complex sediment transport and deposition processes in that specific area, and suggest the influence of local geological events, such as tectonic movements or changes in the surrounding topography, which impacted depositional conditions and led to the formation of inclined lamination. Furthermore, it could also be related to specific diagenetic processes that occurred after deposition, such as compaction or pressure that resulted in the formation of these structures.

Figure 8. Above, X-ray circumferential view, RhoB, Zeff, structure and facies of sample SR-3. Below, plug of the referred sample, showing its textural and structural features. Note in the macroscopic image of the sample the excellent rock selection and some sectors with calcite and kaolinite cement and presence of oxides. The lamination is clearly observed. Source: Authors.
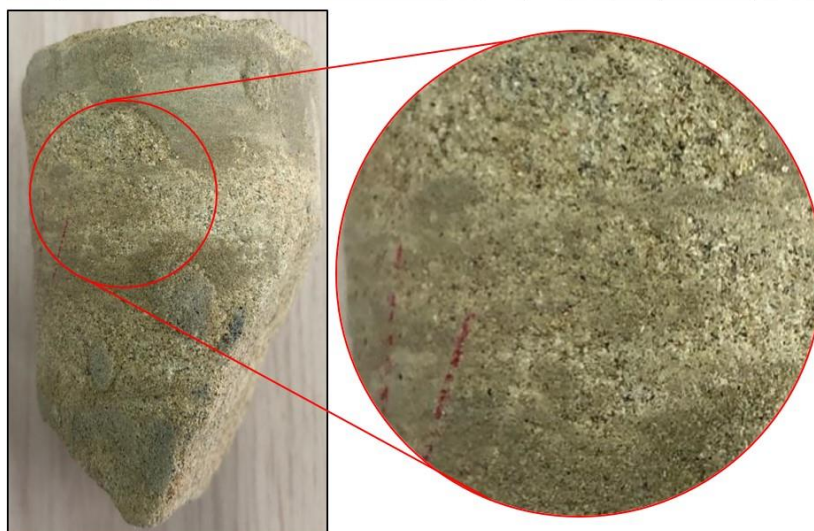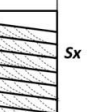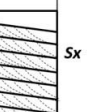

Figure 9. Above, X-ray circumferential view, RhoB, Zeff, structure and facies of sample SR-4. Below, plug of the referred sample, showing its textural and structural features. Note in the macroscopic image of the sample the excellent rock selection and some sectors with calcite cement and presence of oxides. The lamination is clearly observed. Source: Authors.

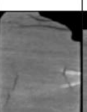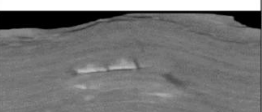In the examined sample SR-5 (Figure 10), two X-ray CT facies have been identified, offering unique insights into the sedimentary characteristics of the rock. The first identified facies, labeled as Slam, exposes the intriguing characteristics of a sandstone adorned with wavy lamination. This revelation suggests a sedimentary history marked by undulating patterns within the sandstone, indicative of fluctuating depositional conditions or unique geological processes that have influenced the formation of this specific facies. The second facies, labeled as Mscon, which is characterized by a sandy mudstone exhibiting convolute deformation, which reveals important information about the geological history and environmental conditions in which the rock was formed. Convolute deformation is characterized by complex and folded folds, creating three-dimensional structures in the rock. It suggests that sedimentation and the accumulation of sediments were neither uniform nor stable, and may indicate dynamic sedimentary conditions, such as fluctuating water currents, tectonic movements, or changes in sediment deposition over time. The formation of convolute deformations is often associated with the presence of water during sediment deposition. It may suggest intermittent periods of water saturation or changes in the water table level during the formation of the rock. Convolute deformation can also result from tectonic forces that affected the region. Movements in the Earth's crust, such as compression or distortion, could have induced the formation of these structures. It can be indicative of significant environmental changes, such as extreme weather events or variations in sediment load. These changes could have influenced the deformation of the rock during or after the sedimentation process.
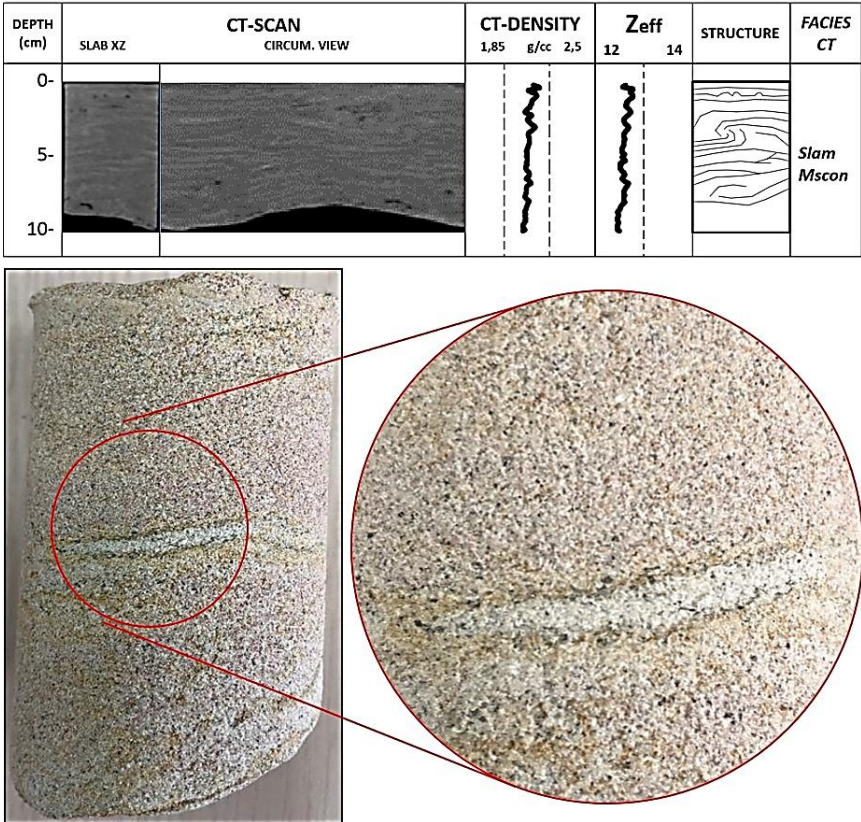
Figure 10. Above, X-ray circumferential view, RhoB, Zeff, structure and facies of sample SR-5. Below, plug of the referred sample, showing its textural and structural features. Note in the macroscopic image of the sample the excellent rock selection and some sectors with calcite cement and presence of oxides. The lamination is clearly observed. Source: Authors.

Beyond elucidating primary sedimentary structures such as laminations, the X-ray CT technique proves instrumental in unraveling the intricacies of syn-sedimentary deformations, which are illustrated in Figs. 7-10. These deformations serve as valuable indicators, offering a profound glimpse into the geological history and processes that shaped the rocks during their formative stages. The high-resolution images acquired through X-ray CT not only provide a comprehensive understanding of syn-sedimentary deformations but also empower researchers to conduct detailed characterizations of stratigraphic sequences. The wealth of information extracted from X-ray CT imagery becomes very important in interpreting the dynamic environmental changes that have unfolded over geological time. By scrutinizing the subtle details captured by the technique, researchers can reconstruct the complex interplay between sedimentary processes and external forces, shedding light on the evolving landscapes and conditions that have shaped the geological framework. In essence, X-ray CT emerges as a versatile tool, not only

enhancing our understanding of primary sedimentary structures but also serving as a gateway to unlocking the multifaceted narratives embedded within the geological record.

The analysis of sedimentary and biogenic structures, along with syn-sedimentary deformations revealed by X-ray CT imaging, serves as a valuable resource in both geological and paleontological research. They assist scientists in documenting and effectively communicating their findings, and the high resolution of the technique allows for detailed identification of these structures, thereby contributing to the advancement of our knowledge about Earth's history and life on it.

On the RhoB and Zeff values, variations are noted that allow to recognize changes, although subtle, in texture and composition, considering the shape of the curves, the scale of the analysis and the size of the samples. For each sample it was possible to assign one or several facies codes, which were recorded in each template, for each sample respectively. Mainly facies of sandstones with inclined trough and straight lamination were recognized, in addition it was possible to identify biogenic structures in some samples. There is not doubt on the significance of the RhoB and Zeff values in characterizing geological samples, particularly in the context of sedimentary rocks. They play a critical role in recognizing even subtle variations in the texture and composition of geological samples. These variations might not be visually obvious but can be quantitatively assessed through these measurements. For instance, changes in mineral composition, porosity, or even the presence of certain elements can be reflected in the RhoB and Zeff data. Different minerals and textures within rocks can lead to distinct shapes in the RhoB and Zeff cross-plot. For example, the presence of denser minerals may result in peaks in the RhoB curve, while variations in mineral composition may lead to shifts in the Zeff curve. Analyzing these curve shapes

can provide insights into the nature of the rock and the changes it has undergone. The scale at which the analysis is conducted plays a significant role in the results. Depending on the scale, variations in RhoB and Zeff may become more or less apparent. Fine-scale analysis allows for the detection of subtle changes that might be overlooked in coarser analyses. This is particularly relevant when studying sedimentary rocks with complex layering and microstructures. Assigning facies codes to each sample is a common practice in sedimentology and geological studies. Facies codes help geologists categorize and describe different rock types or depositional environments within a sedimentary sequence. Each facies code corresponds to a specific set of characteristics, including mineralogy, texture, sedimentary structures, and composition. RhoB and Zeff data have allowed the differentiation of distinct sedimentary features within the rock samples. Sandstone facies often represent specific depositional environments, and their identification contributes to the understanding of the geological history of the area. The ability to identify biogenic structures in some samples is noteworthy. These structures, which result from the activity of organisms, can provide valuable information about past environmental conditions and ecological interactions. Recognizing biogenic structures adds a layer of complexity to the interpretation of sedimentary rocks and can offer insights into ancient ecosystems.

4.2. Petrography
The textural results of the petrography during the counting of all the samples are observed in Table 2. The predominant grain size is medium sand (0.25-0.5 mm). Textures are important features of sandstones; however, their controlling factors are not fully understood. We present a detailed textural analysis of sandstones and discuss the influences of provenance and depositional environments on textures from siliciclastic rocks of the Paleogene La Paz, Esmeralda, Colorado and Mugrosa formations, which are producers of hydrocarbons in the petroleum system from the MMV basin.

Table 2. Textural results from conventional petrography. Source: Authors.

Sample No.	Granule % (2-4 mm)	Very coarse grained sand % (1-2 mm)	Coarse grained sand % (0.5-1 mm)	Middle grained sand % (0.25-0.5 mm)	Fine grained sand % (250-125 μm)	Very fine grained sand % (125-62.5 μm)	Silt % (62.5-3.9 μm)	Clay % (3.9-0.06 μm)
SR-1	0.00	6.67	28.00	44.00	15.33	5.33	0.67	0.00
SR-2	0.00	0.67	18.67	46.00	21.33	12.67	0.67	0.00
SR-3	0.00	0.00	0.00	36.00	36.67	25.33	2.00	0.00
SR-4	0.00	6.00	11.33	30.67	37.33	14.00	0.67	0.00
SR-5	2.00	4.67	9.33	36.67	22.00	18.00	4.00	3.33

There are several schemes of classifying sandstones, but the most commonly used ones incorporate both texture and mineralogy. In this study, we use the classification proposed by Folk [27], which is based on both the relative abundances of quartz (Q), feldspar (F), and lithics (L). Figure 11 shows that the analyzed sedimentary rocks mainly fall into the categories of sublitharenites to subarkoses. This indicates that these rocks are slightly mineralogically mature.

However, there is an exception, sample SR-3, which falls into the field of feldspathic lithoarenites, suggesting a different mineral composition. The main cementing materials found were recrystallized calcite, silica cement and clays, which act as glue, holding the sand grains together in the rock. Evidence of secondary porosity due to dissolution processes of the framework and cement. The porosity is mainly secondary favored by the dissolution of feldspars and lithics mainly. Figures 12-16 show the compositional results of

conventional petrography under a transmitted light microscope of all the samples.
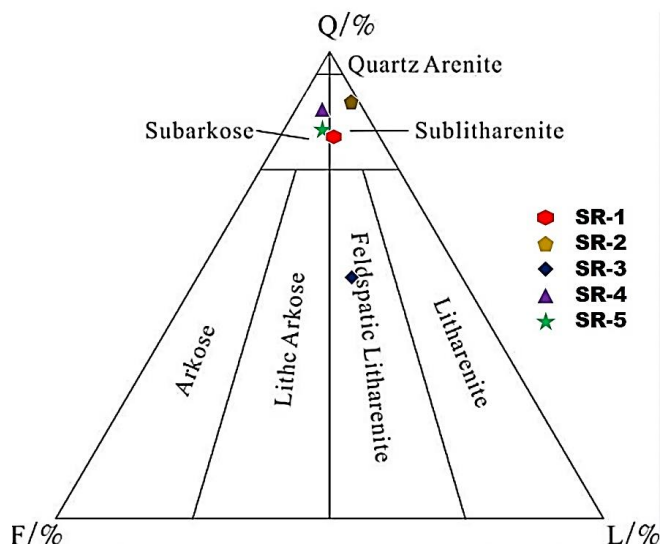

Figure 11. QFL triangular diagram plots [27] of the sedimentary rocks of interest analyzed by means of conventional petrography. Source: Authors.

Figure 12 shows microscopic views (PPL - plane polarized light and XPL - crossed polarized light) of sample SR-1, which is classified as a subarkose and is primarily composed of quartz (81.43%), feldspar (8.57%), and lithic fragments (10.00%). The quartz grains exhibit minor straight wavy extinction and include both monocrystalline and polycrystalline grains of igneous and metamorphic origin. The feldspars are identified as potassium orthoclase variety. Plutonic lithics of felsic composition and sedimentary quartz composition are observed as rock fragments within the sample. This composition may provide insights into the source and geological history of the sandstone. The presence of petrographically undifferentiated clay minerals and silica as overgrowths in quartz grains indicates the presence of interstitial materials. These materials can affect the rock's properties, including its porosity and permeability. The rock exhibits both primary intergranular porosity and secondary porosity due to dissolution processes. The presence of primary porosity suggests that the rock had open spaces between grains even before diagenetic processes occurred. Secondary porosity resulting from dissolution can significantly impact the rock's reservoir characteristics. Conventional petrography analysis indicates that this rock has 6.00% primary porosity and 15.33% total porosity. This information is critical for understanding the rock's suitability for various applications, such as reservoir quality assessment in the oil and gas industry or groundwater aquifer characterization.
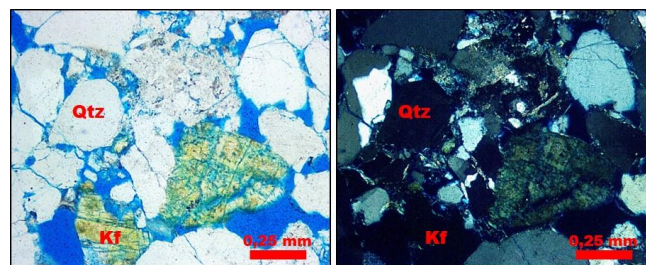

Figure 12. Microscopic views (PPL - plane polarized light and XPL - crossed polarized light) of sample SR-1. Source: Authors.

Figure 13 shows microscopic views (PPL - plane polarized light and XPL - crossed polarized light) of sample SR-2, which is classified as a moderately selected fine sand sublithoarenite and is predominantly composed of quartz (90.34%) and lithic fragments (9.66%). The quartz grains show wavy minor straight extinction and consist of monocrystalline and polycrystalline grains of both metamorphic and igneous origin. Various types of rock fragments, including crypto, micro, and megacrystalline chert, as well as foliated metamorphic lithics with micaceous composition, are observed. The primary interstitial material consists mainly of petrographically undifferentiated clay minerals, along with very low amounts of silica, which are observed as overgrowths in optical and crystallographic continuity with the quartz grains. These interstitial materials can affect the rock's permeability and diagenetic history. The rock exhibits secondary porosity primarily caused by the dissolution of unstable minerals, indicating diagenetic alteration over geological time. Additionally, primary intergranular porosity is also present in the rock. According to conventional petrography, the rock has 3.00% of primary porosity and 18.00% total porosity. The presence of significant secondary porosity is particularly noteworthy, as it may affect the rock's ability to store and transmit fluids such as hydrocarbons or groundwater.

Figure 13. Microscopic views (PPL - plane polarized light and XPL - crossed polarized light) of sample SR-2. Source: Authors.

Figure 14 shows microscopic views (PPL - plane polarized light and XPL - crossed polarized light) of sample SR-3, which is classified as a moderately selected fine sand feldspathic lithoarenite. The rock is composed of quartz (54.61%), feldspar (15.79%), and lithic fragments (29.61%). Notably, the presence of potassium feldspar, quartz, and lithic fragments suggests a diverse source rock or sedimentary history. The presence of non-ferrous calcite filling the rock's porosity indicates a diagenetic process

involving calcite precipitation. This calcite cementation can significantly impact the rock's porosity, permeability, and reservoir quality. The rock contains various constituents, including fragments of foliated metamorphic rock (potentially graphite schist), microcrystalline chert, and clay mineral cement forming coating cements. This complexity suggests a dynamic geological history with multiple phases of sedimentation and diagenesis. The presence of secondary intergranular porosity implies that diagenetic processes have influenced the rock's properties over time. Understanding the nature and extent of this porosity is essential for assessing the rock's capacity to store and transmit fluids. Conventional petrography indicates relatively low porosity, with 3.50% primary porosity and 4.50% total porosity. These values suggest that the rock may not be highly porous, potentially affecting its capacity to store and transmit fluids.
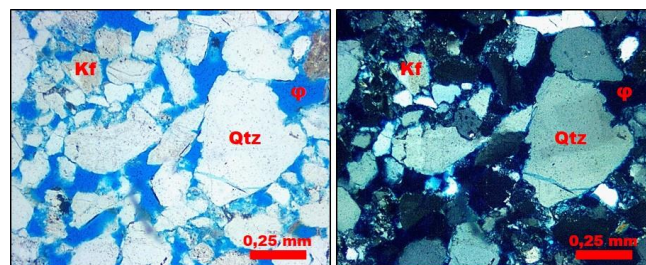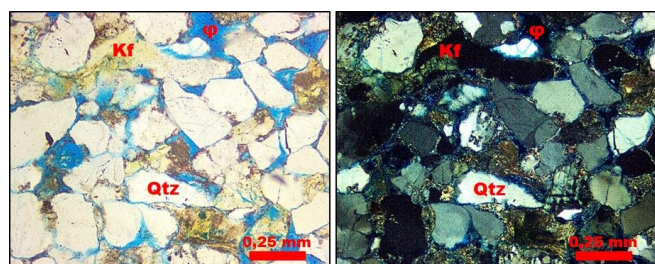

Figure 14. Microscopic views (PPL - plane polarized light and XPL - crossed polarized light) of sample SR-3. Source: Authors.

Figure 15 shows microscopic views (PPL - plane polarized light and XPL - crossed polarized light) of sample SR-4, which is classified as a moderately selected fine sand subarkose. The primary minerals in this rock are quartz (88.75%) and potassium feldspar (6.25%). This mineral composition suggests a sedimentary history influenced by the source material and depositional environment. The presence of detrital grains of potassium feldspar with partial dissolution leading to microporosity is significant. This dissolution process can impact the rock's permeability and fluid flow characteristics. Fragments of intrusive igneous rock (granitoid) are observed within the sample. These fragments can provide insights into the geological history and source rock of the sandstone. The presence of microcrystalline chert grains indicates the diversity of sedimentary components within the rock, potentially reflecting different sediment sources and transport processes. Vermicular kaolinite cement is observed filling the remaining porosity. This cementation process can influence the rock's porosity, permeability, and overall reservoir quality. The presence of intergranular secondary porosity suggests that diagenetic alterations have occurred over time. Understanding the nature and extent of this porosity is fundamental for assessing the rock's suitability for fluid storage and migration. Conventional petrography indicates 5.00% primary porosity and 13.00% total porosity. These values suggest that the rock has significant porosity, which can make it a potential candidate for fluid reservoirs or aquifers.
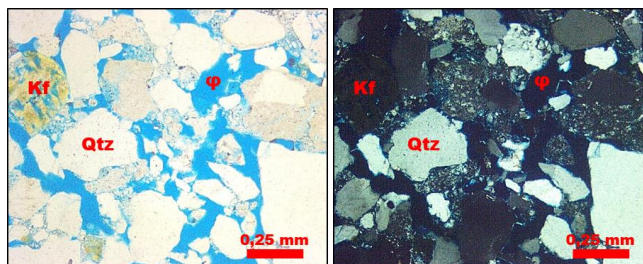

Figure 15. Microscopic views (PPL - plane polarized light and XPL - crossed polarized light) of sample SR-4. Source: Authors.

Figure 16 shows microscopic views (PPL - plane polarized light and XPL - crossed polarized light) of sample SR-5, which is classified as a medium to coarse-grained sublithosandrite with moderate sorting. It consists of subangular to subrounded grains in tangential to linear contact, with a mineral composition primarily comprising 84.62% quartz, 5.77% feldspar, and 9.62% lithic fragments. The quartz grains exhibit predominantly straight extinction and are mostly monocrystalline, although moderate amounts of wavy extinction quartz can be distinguished. Polycrystalline quartz is mainly of the diffuse igneous type, with some foliated polycrystalline quartz present. Microcrystalline chert is observed in low amounts, and there is a negligible content of heavy minerals such as tourmaline and zircon. The grains are embedded in a depositional matrix of petrographically undifferentiated clay minerals, with some sectors showing alteration to sericite. Petrographic porosity is high, mainly comprising mesopores, micropores, and smaller megapores, primarily of secondary origin due to the dissolution of the clayey matrix. Conventional petrography results indicate that this rock has 2.50% primary porosity and 7.50% secondary porosity. The high secondary porosity suggests that this sample may have potential as a fluid reservoir, such as for oil or gas. The combination of predominantly monocrystalline quartz and diffuse igneous polycrystalline quartz could influence its fluid storage and conductivity capacity. The presence of matrix sectors altered to sericite indicates that the rock has undergone geological changes at a later stage. This could be relevant for understanding the geological history of the region and the tectonic or diagenetic processes that affected it. The absence of heavy minerals like tourmaline and zircon could be relevant for interpreting past sediment transport and deposition conditions. The abundance of quartz and the presence of feldspar and lithic fragments suggest a possible sedimentary origin for this rock. This could provide information about the deposition environment and the geological history of the region.
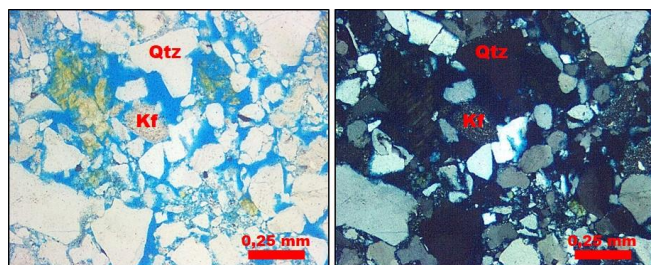
Figure 16. Microscopic views (PPL - plane polarized light and XPL - crossed polarized light) of sample SR-5. Source: Authors.

4.3. X-ray diffraction

Figure 17 presents the XRPD patterns obtained from the analyzed sandstone samples, revealing their crystalline mineral phases through XRPD. All quartz and a corundum standard (α-phase) with which quantitative analysis can be performed signals are highlighted. XRPD patterns reveal the occurrence of quartz at $21.4o$ of 2θ and other signs, corresponding to feldspars at $23.5o$ 2θ and clay minerals, which are located between 3.5 and $34.0o$ of 2θ. It is emphasized that the analyzed sandstones present detection of muscovite signals. Montmorillonite at $8.8o$ of 2θ, which in basal spacing d can be 9.99 Å was observed in samples SR-1

and SR-3. Kaolinite is characterized by the signals at 12.5 and $6.2o$ of 2θ. For the analyzed sandstones, more signals attributed to kaolinite stand out. All samples present muscovite and kaolinite in the region previously indicated. No interstratified signals have been detected, and, in summary, the samples have different amounts of muscovite and clay minerals, feldspars and abundant quartz. SR-1 is composed of quartz (69.7%), albite (9.6%), microcline (8.8%), muscovite (4.6%), montmorillonite (4.3%), kaolinite (3.0%), and traces of orthoclase, clinochlore and hematite. SR-2 consists mainly of quartz (98.0%), minor kaolinite (1.7%) and traces of muscovite, crystoballite, anatase and pyrite. SR-3 is composed of quartz (72.3%), microcline (6.8%), montmorillonite (6.3%), muscovite (5.8%), kaolinite (5.4%), albite (9.6%), and traces of anatase, hematite, calcite and Ca-albite. SR-4 consists mainly of quartz (95.3%), minor microcline (2.3%), kaolinite (1.7%) and traces of muscovite, crystoballite and anatase. SR-5 consists mainly of quartz (96.0%), minor microcline (2.2%), kaolinite (1.4%) and traces of muscovite, crystoballite and anatase. Additional low intensity reflections were observed that could not be assigned to any phases reported in the PDF-2 database.
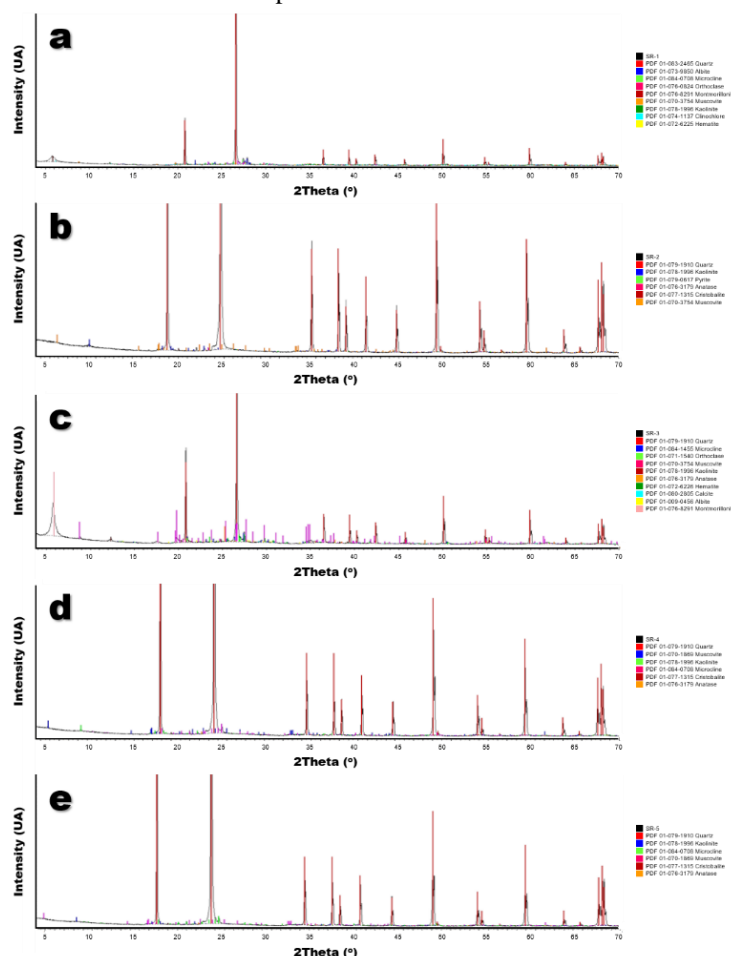

Figure 17. X-ray diffraction patterns of the analyzed sandstones. (a) SR-1, (b) SR-2, (c) SR-3, (d) SR-4 and (e) SR-5. Source: Authors.
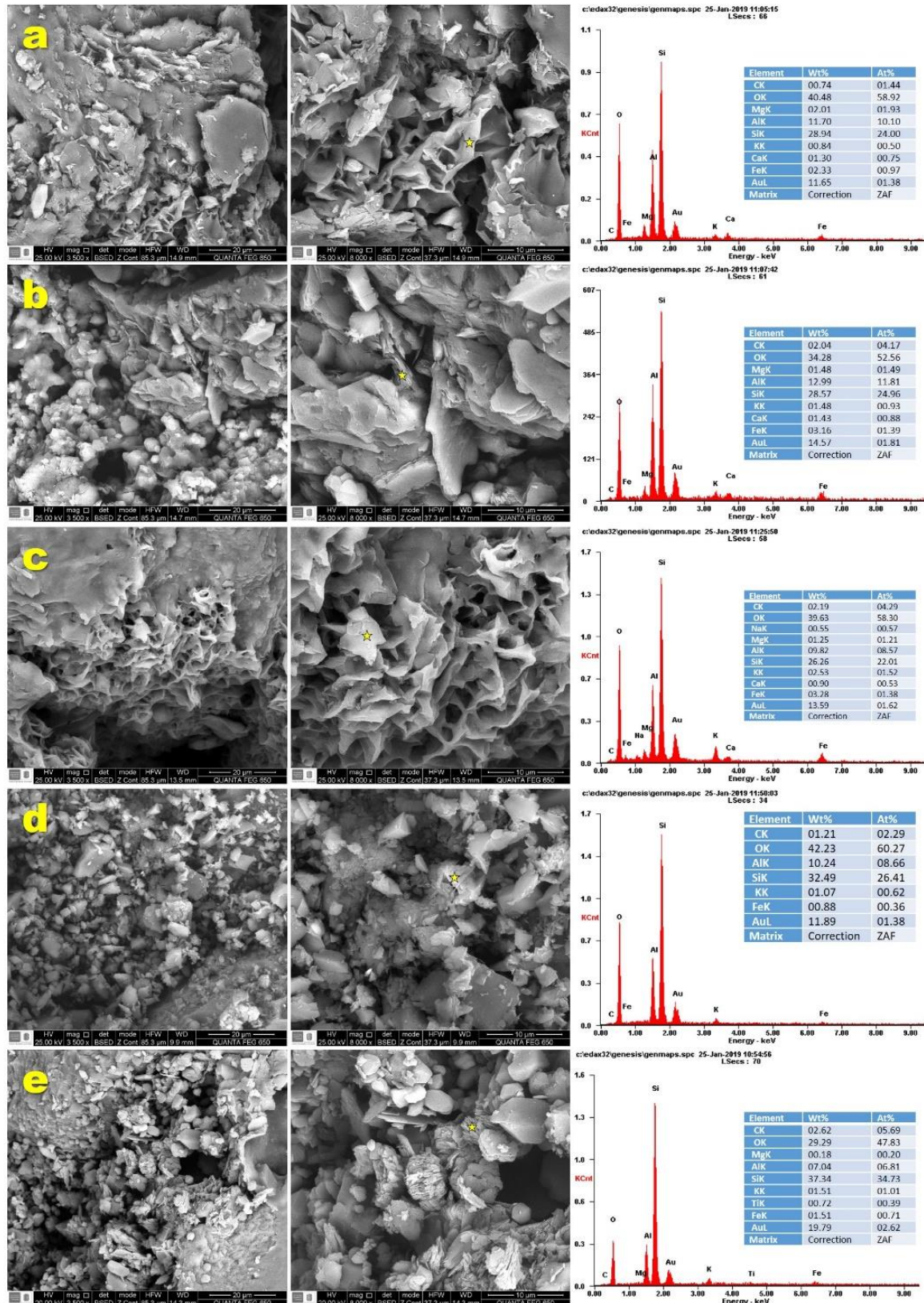
Figure 18. SE images and EDS spectrum of the typical clay mineral phases present in the analyzed sandstones. (a) SR-1, (b) SR-2, (c) SR-3, (d) SR-4 and (e) SR-5. Source: Authors.

4.4. Scanning electron microscopy

Through the application of SEM/EDS analysis, it is possible to look down into the pores, identify the smallest minerals and examine their distribution within the pores. Figure 18 shows the microstructure of analyzed sandstones with different grain sizes measured using Backscattered electron (SE) images, which reveal some differences. The sample SR-1 (Figure 18a) has a dense structure, clear boundaries, many pores, medium degree of cementation, abundant clay minerals (mainly montmorillonite and minor kaolinite) and quartz surrounded very closely by clay minerals. The sample SR-2 (Figure 18b) is a coarse-grained sandstone, to difference it of others with similar grain size is that it not present high content of matrix. In the porous spaces presents kaolinite in discrete particles, microscrystalline quartz. Kaolinite can give an effect inside of porous for generating microporosities, but it does not show a significant damage on formation; however, montmorillonite brigding-pore is a morphology that not impact in the porosity but your effects in the permeability is a serious damage on formation [38]. This sandstone has a loose structure, very clear boundaries, numerous pores, and the least degree of cementation, very few clay minerals and quartz surrounded very sparsely by clay minerals. The sample SR-3 (Figure 18c) presents the more beautiful autigenic clay in our samples. En overview, presents a coarse-grained particle, with fractures and porous with clay minerals (kaolinite and montmorillonite). It is possible to observe authigenic kaolinite with a pseudo-vermicular form and goethite in concentric chopsticks-like of 2 µm. The sample SR-4 (Figure 18d) has a very dense structure, fuzzy boundaries, few pores, the highest degree of cementation, minor clay minerals (kaolinite) and abundant quartz surrounded very closely by clay minerals. The sample SR-5 (Figure 18e) presents a coarse-grained sandstone and in addition, quite matrix with plagioclase altered to sericite. In the pores, there are clay minerals and microcrystalline quartz. This autigenic quartz cement is a form of pore-occluding mineral in deeply buried sandstone, approximately >2500 meters and is an important to considerer that some deeply buried reservoirs contain more porosity that predicted by existing conceptual models of quartz cementation [39].

5. Discussion

X-ray CT has emerged as an indispensable tool in the study of sedimentary rocks, driven primarily by the evolving needs of the oil industry. The assessment of rock cores, particularly sedimentological evaluations, often limits the availability of samples for further necessary and specialized analyses. Furthermore, traditional methods are often time-consuming and resource-intensive [40]. Therefore, non-destructive analytical techniques have gained prominence in the investigation of petrophysical properties of sedimentary rocks, enabling the acquisition of substantial quantities of high-quality data without compromising the sample integrity. Among these techniques, it stands out, which represents a non-invasive exploration method that uses X-rays to take images in both 2D and 3D following the spatial planes that are considered, and which has had a boom in recent years. years, evidenced in multiple scientific and technological advances.

The proposed workflow showed positive results, considering that it allowed a previous interpretation and recognition of sedimentological characteristics in each sample studied. X-ray CT's unique capabilities extend to the precise identification of sedimentological characteristics within rock samples, which includes the discernment of primary, secondary, and biogenic sedimentary structures. The ability to visualize these structures facilitates the approximation of deposition conditions and the nature of the transporting agent. When coupled with macroscopic descriptions, X-ray CT supports the identification of facies, offering valuable insights into the sedimentological attributes of the deposit and the broader sedimentary environment [41].

X-ray CT provides RhoB and Zeff information, effectively harnessing this data for sedimentological interpretation remains a challenge [42]. These values represent thae summation of physical characteristics within a defined rock volume. Quantitative and qualitative studies are imperative to correlate RhoB and Zeff values with the petrographic characteristics of the rock volume. Such investigations should strive to establish direct relationships between these properties and sedimentological features.

To maximize the utility of X-ray CT in sedimentological interpretation, it is advisable to use it in conjunction with traditional methods such as petrography [27,43], X-ray diffraction [44], scanning electron microscopy [45], and others [46-49]. This interdisciplinary approach can help establish robust criteria for sedimentological analysis and enhance the recognition of deposition characteristics that provide insights into sedimentary deposit formation conditions.

While examining the samples, a clear pattern emerges regarding the behavior of RhoB and Zeff curves in relation to the preservation of sedimentary structures. In instances where the sedimentary structures appear diffuse or relict, we consistently observe a similar trend in the curves, characterized by lower values. This suggests that the presence of these diffuse or relict structures may have contributed to a decrease in RhoB and Zeff. In stark contrast, when sedimentary structures are well-preserved, the curves exhibit more variable behaviors, often displaying higher values. This phenomenon hints at a potential link between the preservation of sedimentary structures and an increase in RhoB and Zeff. Notably, our findings also indicate distinct differences between samples with varying compositions. Samples classified as sublitharenite (e.g., SR-1 and SR-2)

consistently exhibit lower RhoB and Zeff values compared to those categorized as subarkose (e.g., SR-4 and SR-5). Conversely, the sample with a feldspathic lithoarenite composition, SR-3, records the highest values for both RhoB and Zeff (as illustrated in Figs. 5-9). When we cross-reference these observations with the results of conventional petrography (as shown in Figs. 11-15), a notable trend becomes apparent. Samples with lower RhoB and Zeff values, such as SR-1 and SR-2, have experienced more significant grain dissolution and exhibit an increase in secondary porosity. Conversely, samples with fewer dissolved grains, like SR-3, SR-4, and SR-5, tend to register higher RhoB and Zeff values alongside a decrease in secondary porosity. It is important to highlight that our sample selection prioritized medium sand (0.25-0.5 mm) predominance to minimize the potential influence of grain size. While these findings emphasize the utility of X-ray CT as a valuable tool for characterizing sedimentary materials, it is important to note that its precise role in sedimentological interpretation remains a subject of ongoing exploration. To establish a more comprehensive understanding, future studies should aim to establish direct quantitative and qualitative relationships between X-ray CT data and sedimentological characteristics. As shown, X-ray CT is a highly useful tool, but its role in sedimentological interpretation remains difficult to define at this stage. Further studies are needed to establish direct relationships between quantitative and qualitative results. Therefore, it is recommended to use X-ray CT as a complementary tool alongside petrography, XRPD, SEM, and other techniques, to establish criteria for sedimentological analysis and identify depositional features that provide evidence of the conditions under which sedimentary deposits formed.

6. Conclusions

The multi-analytical approach employed in this study provides a comprehensive understanding of the Paleogene sedimentary rocks in the MMV basin by combining advanced imaging and traditional analytical methods. X-ray CT proved to be a valuable non-destructive technique, delivering high-resolution images that facilitate the identification of sedimentary structures, biogenic features, and syn-sedimentary deformations. When integrated with conventional methods such as petrography, XRPD, and SEM, this approach yields a more complete insight into the sedimentological and petrophysical characteristics of the samples.

RhoB and Zeff values derived from X-ray CT emerged as key indicators for differentiating sedimentary features, reflecting variations in texture and composition within the rocks. The facies codes recognized from the X-ray CT data showed strong agreement with petrographic observations,

highlighting the potential of this technique for facies identification and classification. Moreover, the analysis of primary sedimentary structures like laminations and the detection of syn-sedimentary deformations contributed significantly to reconstructing the geological history of the region. This combined approach enabled the identification of multiple facies within the studied rock formations, illustrating the utility of X-ray CT in sedimentological analysis.Petrographic examination revealed that the sandstones are predominantly medium-grained, exhibiting variations in cementing materials and secondary porosity. Utilizing Folk's classification scheme allowed for an understanding of the mineralogical maturity of the rocks, which ranges from low to medium. The presence of both primary and secondary porosity, as identified through petrography, has important implications for reservoir quality and fluid flow characteristics, key factors in resource exploration and exploitation.

XRPD analysis complemented these findings by detailing the mineralogical composition, with quartz, feldspars, and various clay minerals such as muscovite and montmorillonite being prominent. The detection of these clay minerals contributes to a deeper understanding of the diagenetic processes affecting the sandstones. SEM further enhanced this mineralogical insight by revealing microstructural features, including the distribution of clay minerals within pore spaces and their influence on porosity and permeability.

Correlating data from X-ray CT, petrography, XRPD, SEM, and petrophysical analyses uncovered significant relationships. In particular, the preservation of sedimentary structures was found to directly influence petrophysical properties such as density and effective atomic number, underscoring the interconnected nature of the rock's textural and physical attributes.

While the study delivers valuable insights into the sedimentology and petrophysics of the MMV basin sandstones, it also recognizes the need for future research. Further work should aim to establish more direct and quantitative correlations between X-ray CT data and sedimentological parameters, enhancing the predictive power of this technique. Overall, the application of X-ray CT as a complementary tool, combined with other analytical methods, remains essential for advancing a comprehensive understanding of sedimentary deposits and their reservoir potential.

Acknowledgments

References

[1] Kamath, J., Xu, B., Lee, S.H., Yortsos, Y.C. Use of pore network models to interpret laboratory experiments on vugular rocks. Journal of Petroleum Science and Engineering, 20(3-4) (1998) 109-115. https://doi.org/10.1016/S0920-4105(98)00009-6

[2] Ueta, K., Tani, K., Kato, T. Computerized X-ray tomography analysis of three-dimensional fault geometries in basement-induced wrench faulting. Developments in Geotechnical Engineering 84 (2000) 233-246. https://doi.org/10.1016/S0165-1250(00)80019-X

[3] Akin, S., Kovscek, A.R. Computed tomography in petroleum engineering research. In: Mees, F., Swennen, R., Van Geet, M., Jacobs, P. (eds.). Application of X-ray Computed Tomography in the Geosciences, Geological Society of London, Special Publications, 215 (2003) 23-38.

[4] Mees, F., Swennen, R., Geet, M.V., Jacobs, P. Applications of X-Ray Computed Tomography in Geosciences. Geological Society of London, Special Publications, 215 (2003) 1-6. https://doi.org/10.1144/GSL.SP.2003.215.01.01

[5] Földes, T., Árgyelán, G.B., Bogner, P., Repa, I., Kiss, B., Hips, K. Application of medical Computer Tomograph measurements to 3D reservoir characterization. Acta Geologica Hungarica, 47(1) (2004) 63–73. https://doi.org/10.1556/AGeol.47.2004.1.5

[6] Siddiqui, S., Khamees, A.A. Dual-Energy CT-Scanning Applications in Rock Characterization. SPE Annual Technical Conference and Exhibition, Houston, USA, September 26-29, 2004. SPE 90520-MS.

[7] Cnudde, V., Boone, M.N. High-resolution X-ray computed tomography in geosciences: a review of the current technology and applications. Earth-Science Reviews, 123 (2013) 1–17. https://doi.org/10.1016/j.earscirev.2013.04.003

[8] Mena, A., Francés, G., Pérez-Arlucea, M., Aguiar, P., Barreiro-Vázquez, J.D., Iglesias, A., Barreiro-Lois, A. A novel sedimentological method based on CT-scanning: Use for tomographic characterization of the Galicia Interior Basin. Sedimentary Geology, 321 (2015) 123-138. https://doi.org/10.1016/j.sedgeo.2015.03.007

[9] Al-Marzouq, A.M., Al-Ghamdi, T.M., Koronfol, S., Dernaika, M.R., Walls, J.D. Shale Gas Characterization and Property Determination by Digital Rock Physics, SPE-SAS Annual Technical Symposium & Exhibition, Al Khobar, Saudi Arabia, April 21-24, 2014.

[10] Walls, J.D., Sinclair, S.W. An Integrated Approach to Shale Reservoir Characterization Using Digital Rock Physics. 12th International Congress of the Brazilian Geophysical Society, Rio de Janeiro, Brazil, August 15-18, 2011.

[11] Van Geet, M., Swennen, R., Wevers, M. Towards 3-D petrography: application of microfocus computer tomography in geological science. Computers & Geosciences 27 (2001) 1091-1099. https://doi.org/10.1016/S0098-3004(00)00154-0

[12] Mogensen, K., Stenby, E.H., Zhou, D. Studies of waterflooding in low-permeable chalk by use of X-ray CT scanning. Journal of Petroleum Science and Engineering, 32(1) (2001) 1-10. https://doi.org/10.1016/S0920-4105(01)00143-7

[13] Anderson, S.H., Gantzer, C.J., Boone, J.M. Rapid non-destructive bulk density and soil water content determination by computer tomography. Soil Science Society of America Journal, 52 (1988) 35-40. https://doi.org/10.2136/sssaj1988.03615995005200010006x

[14] Renter, J.A.M. Applications of computerized tomography in sedimentology. Marine Geotechnology, 8(3) (1989) 201-211. https://doi.org/10.1080/10641198909379868

[15] Baniak, G.M., Gingras, M.K., Pemberton, S.G. Reservoir characterization of burrow-associated dolomites in the upper Devonian Wabamun group, Pine Creek gas field, central Alberta, Canada. Marine and Petroleum Geology, 48 (2013) 275–292. https://doi.org/10.1016/j.marpetgeo.2013.08.020

[16] Deprez, M. Multiscale micro-CT imaging on sediment cores: unravelling the paleoflow directions in a megaturbidite (Lake Lucerne, Switzerland). Master thesis, Universiteit Gent, Gent, Belgium (2016).

[17] Liu, X., Wang, J., Ge, L., Hu, F., Li, C., Li, X., Yu, J., Xu, H., Lu, S., Xue, Q. Pore-scale characterization of tight sandstone in Yanchang Formation Ordos Basin China using micro-CT and SEM imaging from nm- to cm-scale. Fuel, 209 (2017) 254-264. https://doi.org/10.1016/j.fuel.2017.07.068

[18] García, A.G., Marín, D.A. Estado del Arte del Uso de la Física Digital de Rocas para la Caracterización en Medios Porosos. Undergraduate Thesis, Universidad Industrial de Santander, Bucaramanga, Colombia (2018).

[19] Caballero, V., Parra, M., Mora, A.R. Levantamiento de la Cordillera Oriental durante el Eoceno tardío – Oligoceno temprano Proveniencia sedimentaria en el sinclinal de Nuevo Mundo cuenca Valle Medio del Magdalena. Boletín de Geología, 32(1) (2010) 45–77.

[20] Gómez, E., Jordan, T., Allmendinger, R. Syntectonic Cenozoic sedimentation in the northern Middle Magdalena Valley Basin of Colombia and implications for exhumation of the Northern Andes. Geological Society of America Bulletin, 117(5) (2005) 547–569. https://doi.org/10.1130/B25454.1

[21] Sarmiento, G., Puentes, J., Sierra, C. Evolution of the geological and stratigraphic framework of the northern sector of the Middle Magdalena Valley. Geología Norandina 12 (2015) 51-58.

[22] Velandia, F. Kinematics of the major faults of the Santander Massif: emphasis on the structural model and temporality south of the Bucaramanga Fault. PhD Thesis, Universidad Nacional de Colombia, Bogotá, Colombia (2017).

[23] INGEOMINAS. Mapa geológico del cuadrángulo H-12, Bucaramanga - Colombia. Bogotá: Instituto Nacional de Investigaciones Geológicas y Mineras - INGEOMINAS (1969).

[24] Barrero, D., Pardo, A., Vargas, C., Martínez, J. Colombian sedimentary basins: Nomenclature, boundaries and petroleum geology, a new proposal. Agencia Nacional de Hidrocarburos (2007).

[25] Reineck, H.E. Parameter von Schichtung und bioturbation. Geologischen Rundschau, 56 (1967) 420-438. https://doi.org/10.1007/BF01848734

[26] Taylor, A.M., Goldring, R. Description and analysis of bioturbation and ichnofabric. Journal of the Geological Society of London, 150 (1993) 141-148. https://doi.org/10.1144/gsjgs.150.1.014

[27] Folk, R.L. Petrology of Sedimentary Rocks. Hemphill Publishing Co., Austin (1974).

[28] Pettijohn, F.J. Sedimentary Rocks. Harper and Row Publishers, New York (1975).

[29] Limarino, C., Caselli, A., Net, L., Gagliardo, M. A propose of sepfite classification relationed to sand and sandstones composition. Asociación Argentina de Sedimentología, Buenos Aires (1996).

[30] Choquette, P.W., Pray, L.C. Geologic Nomenclature and Classification of Porosity in Sedimentary Carbonates. American Association of Petroleum Geologists Bulletin, 54(2) (1970) 207-250. https://doi.org/10.1306/5D25C98B-16C1-11D7-8645000102C1865D

[31] Picard, M.D. Classification of fine-grained sedimentary rocks. Journal of Sedimentary Research, 41(1) (1971) 179-195. https://doi.org/10.1306/74D7221B-2B21-11D7-8648000102C1865D

[32] Boggs, S. Principles of sedimentology and stratigraphy. Prentice Hall, Hoboken (2006).

[33] Winkler, E.M. Stone: Properties, Durability in Man's Environment. Springer-Verlag, New York (1973).

[34] Johnson, G.R., Olhoeft, G.R., Carmichael, R.S. Density of rocks and minerals. In: Carmichael, R.S. (eds.). Handbook of Physical Properties of Rocks, CRC Press (1984) 1-38.

[35] Komar, P.D. Selective gravel entrainment and the empirical evaluation of flow competence. Sedimentology, 34 (1987) 1165-1176. https://doi.org/10.1111/j.1365-3091.1987.tb00599.x

[36] Wellington, S.L., Vinegar, H.J. X-Ray Computerized Tomography. Journal of Petroleum Technology 39 (1987) 885–898. https://doi.org/10.2118/16983-PA

[37] Siddiqui, S. Some Useful Guidelines for Whole Core CT-Scanning for Petrophysical Applications. International Symposium of the Society of Core Analysts, Houston, USA, September 19-22, 2022. https://doi.org/10.1051/e3sconf/202336701013.

[38] Kantorowicz, J.D. The influence of variations in illite morphology on the permeability of Middle Jurassic Brent Group sandstones, Cormorant Field, UK North Sea. Marine and Petroleum Geology, 7(1) (1990) 66–74. https://doi.org/10.1016/0264-8172(90)90057-N

[39] French, M.W., Worden, R.H., Mariani, E., Larese, R.E., Mueller, R.R., Kliewer, C.E. Microcrystalline Quartz Generation and the Preservation of Porosity in Sandstones: Evidence from the Upper Cretaceous of the Subhercynian Basin, Germany. Journal of Sedimentary Research 82 (2012) 422-434. https://doi.org/10.2110/jsr.2012.39

[40] Menke, W. Geophysical Data Analysis: Discrete Inverse Theory. Academic Press, New York (2018).

[41] Machel, H.G. Concepts and models of dolomitization: A critical reappraisal. Geological Society of London, Special Publications, 235(1) (2004) 7-63. https://doi.org/10.1144/GSL.SP.2004.235.01

[42] Loucks, R.G., Ruppel, S.C. Mississippian Barnett Shale: Lithofacies and Depositional Setting of a Deep-Water Shale-Gas Succession in the Fort Worth Basin, Texas. American Association of Petroleum Geologists Bulletin, 91(4) (2007) 579–601. https://doi.org/10.1306/11020606059

[43] Kasim, S.A., Ismail, M.S., Ahmed, N., Rashid, A. Facies analysis, petrography and textural characteristics of the onshore Paleogene-Neogene Lawin Basin, Perak, Peninsular Malaysia: Insights into palaeodepositional environment and provenance. Journal of Asian Earth Sciences: X 9 (2023) 100150. https://doi.org/10.1016/j.jaesx.2023.100150

[44] Šujan, M., Aherwar, K., Vojtko, R., Braucher, R., Šarinová, K., Chyba, A., Hók, J., Grizelj, A., Pipík, R., Lalinská-Voleková, B., Rózsová, B., Team, A. Stratigraphic, sedimentological, geochemical, mineralogical and geochronological data characterizing the Upper Miocene sequence of the Turiec Basin, Western Carpathians (Central Europe). Data Brief 52 (2024) 109810. https://doi.org/10.1016/j.dib.2023.109810

[45] Al-Ojaili, W.A.Q., Shalaby, M.R., Bauer, W. Reservoir quality evaluation of the Narimba Formation in Bass Basin, Australia: Implications from petrophysical analysis, sedimentological features, capillary pressure and wetting fluid saturation. Energy Geoscience, 5(1) (2024) 100220. https://doi.org/10.1016/j.engeos.2023.100220

[46] Blatt, H., Middleton, G., Murray, R. Origin of Sedimentary Rocks. Prentice-Hall, New Jersey (1980).

[47] Fallatah, M.I., Alnazghah, M., Kerans, C., Al-Hussaini, A. Sedimentology and carbon isotope stratigraphy from the Late Jurassic – Early Cretaceous of the Arabian plate: The Weissert event and the VOICE in the Tethys Realm? Marine and Petroleum Geology 161 (2024) 106670. https://doi.org/10.1016/j.marpetgeo.2023.106670

[48] Ferreira, L.d.O., Chagas, V.E., Bobco, F.E.R., de Souza, D.C., Salgado-Campos, V.M.J., Sedorko, D., Neves, M., Silveira, L.F., Mendonça Filho, J.G., Araújo, B.C., Borghi, L. Tracking environmental changes in an Early Cretaceous epicontinental sea: Sedimentology and geochemistry of the Romualdo Formation (Araripe Basin, NE Brazil). Cretaceous Research 166 (2025) 105986. https://doi.org/10.1016/j.cretres.2024.105986

[49] Mohammadi, Z., Capezzuoli, E., Claes, H., Alipoor, R., Muchez, P., Swennen, R. Substrate geology controlling different morphology, sedimentology, diagenesis and geochemistry of adjacent travertine bodies: A case study from the Sanandaj-Sirjan zone (western Iran). Sedimentary Geology 389 (2019) 127-146. https://doi.org/10.1016/j.sedgeo.2019.06.005